Chapter 5

Results

The significance of this work is the creation of a four-wheeled vehicle modelling technique that is designed to be used throughout a total suspension design. The rest of this chapter is the presentation of results obtained from a computer implementation of this model. During the final stages of the analysis, the solution technique was found to be unstable when the equations became increasingly non-linear or close to the linear threshold. These results are not included in this chapter. Solution stability is addressed in section 5.4.

5.1 Vehicle Parameters for a Combined Maneuver Analysis

The vehicle model developed in Chapter Three is coded into a computer program in Chapter Four using a Newton-Raphson solution technique. The vehicle equations are developed in a general manner to facilitate the total suspension design process. However, only one specific vehicle is selected to exercise the vehicle model. The computer model is executed using input parameters representing a small commuter vehicle; proprietary privilege prevents any further description. The results are compared to existing data from [3] to predict the applicability of the model and direct further development.

The minimum number of vehicle parameters necessary to analyze

the model are listed in Table 2. The total number of parameters needed increases when the suspension and tire models become more complex. This demonstrates the major strength of this particular model. The analysis can start with basic parameters and become more comprehensive as the vehicle design is further defined.

Table 2

Vehicle Parameters For Analysis

Symbol	Description	Units	Test Value
BP	FRACTION OF BRAKING AT FRONT....	(UNITLESS)	0.7
CALPHAB	BACK LATERAL TIRE STIFFNESS.....	(N/RAD)	48415.0
CALPHAF	FRONT LATERAL TIRE STIFFNESS.....	(N/RAD)	35683.0
DRVAXL$	RWD OR FWD SPECIFIER.....	(UNITLESS)	RWD
H	SPINDLE TO CG VERT DISTANCE AT DESIGN.	(CM)	20.0*
IXZ	MASS CROSS PROD OF INERTIA .	((kg/100)CM^2)	3600.0
IYZ	MASS CROSS PROD OF INERTIA .	((kg/100)CM^2)	500. EST.
IZZ	MASS MOM OF INERTIA ABOUT Z	((kg/100)CM^2)	1.406E05
KB	BACK SPINDLE RATE PER WHEEL	(N/CM)	362.0
KF	FRONT SPINDLE RATE PER WHEEL	(N/CM)	144.0
KPB	BACK ROLL RATE DUE TO STAB. BAR	(N/CM)	0.0
KPF	FRONT ROLL RATE DUE TO STAB. BAR ...	(N/CM)	148.89
KTB	BACK RADIAL TIRE RATE PER TIRE	(N/CM)	1930.0
KTF	FRONT RADIAL TIRE RATE PER TIRE	(N/CM)	1930.0
L1	DISTANCE FROM C.G. TO FRNT WHEEL.....	(CM)	136.7
L2	DISTANCE FROM C.G. TO REAR WHEEL.....	(CM)	100.5
M	MASS OF THE SPRUNG MASS.....	(KG/10)	11.78
TB	BACK TRACK WIDTH	(CM)	149.2
TF	FRONT TRACK WIDTH	(CM)	146.8

* as modified in section 3.3

5.2 Pure Cornering Analysis to Predict Steer Characteristics

Pure cornering analysis is performed to assure the model predicts the appropriate understeer behavior when the weight distribution is drastically changed. The first vehicle simulation configuration uses the parameters in Table 2 and a linear tire model, equation (3-58). The suspension model is also linear and therefore contains no anti-feature effects. When the vehicle moves around a constant radius curve of 30 meters, several vehicle quasi-static positions are calculated as the steady-state velocity is increased. This situation is simulated with three different weight distributions by altering the L1 and L2 parameters (see L1 and L2 in Figure 3-4) as follows:

1) as prescribed in Table 2 L1 = 136.7cm, L2 = 100.5cm;

2) moving the C.G. forward L1 = 100.5cm, L2 = 136.7cm; and

3) moving the C.G. rearward L1 = 173.4cm, L2 = 63.8cm.

Figure 5-1 shows a plot of steer angle vs steady-state speed for these three situations. The result from the simulation compares favorably with the expected result given by the plot from [3] shown in Figure 5-2. The vehicle with the weight biased forward understeers at the limit and the rear biased vehicle oversteers at the limit. This is also expected based on the explanation of steer characteristics in Chapter Two. The results from Figure 5-1 show the prescribed L1 and L2 parameters in Table 2 make the vehicle nearly neutralsteering. In fact, most domestic cars are designed for slight understeer at the limit for best perceived handling characteristics; this car slightly oversteers.

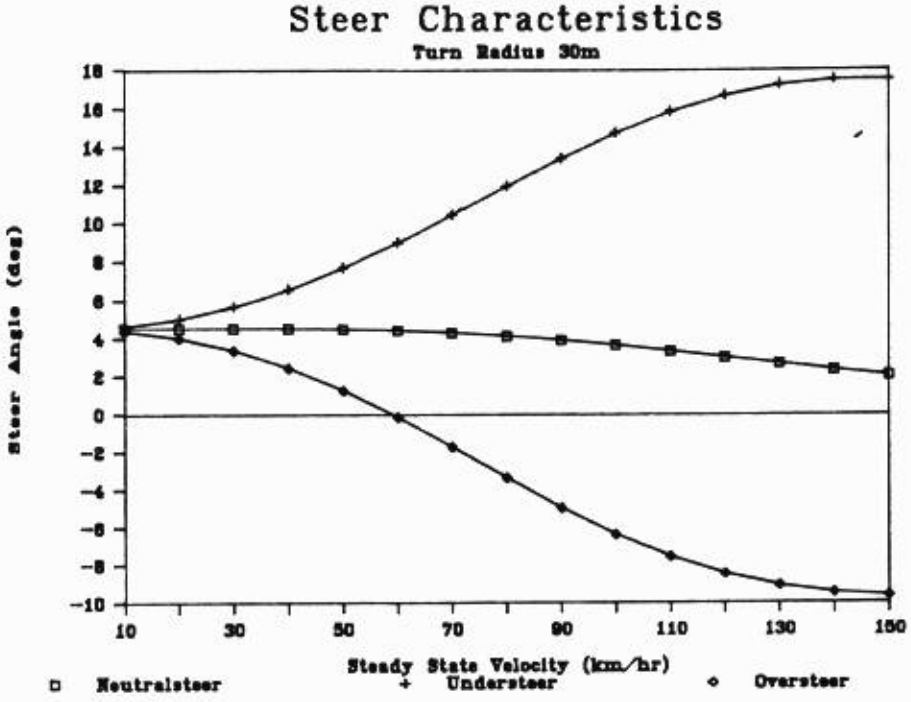

Figure 5-1 Weight distribution effect on steering - predicted

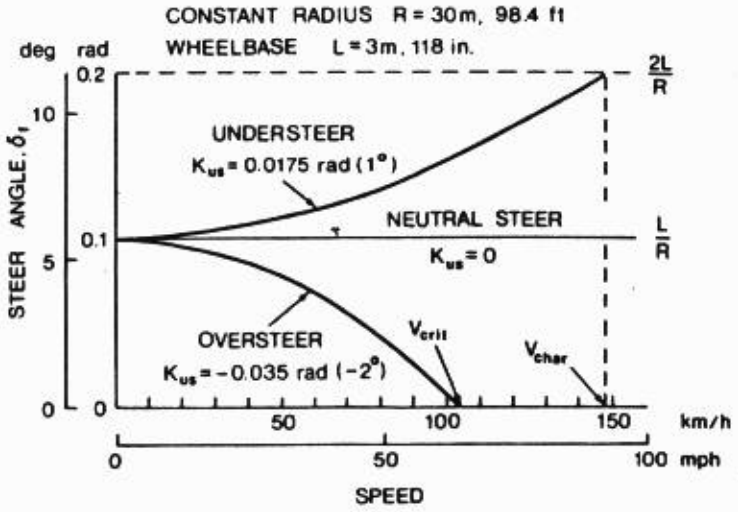

Figure 5-2 Vehicle steer characteristics - Wong [3]

Figure 5-3 shows a plot of yaw gain vs steady-state velocity for the three situations simulated. Yaw gain is the yaw velocity divided by the steer angle and is used to compare steer induced steady-state response from one vehicle to another. By changing the weight distribution of the vehicle described above, a new vehicle is effectively created. Again, the simulated results correlate well with the expected results from [3] shown in Figures 5-3 and 5-4 respectively.

Finally, vehicle steady-state handling characteristics are also compared using a parameter called the understeer coefficient defined in [3]. This parameter is generated by Wong in the form:

$$K_{US} = \frac{W_F}{C_{AF}} - \frac{W_R}{C_{AR}} \qquad (5\text{-}1)$$

However, by making the substitution:

$$W_F = \frac{W\ L2}{(L1 + L2)} \quad \text{and} \quad W_R = \frac{W\ L1}{(L1 + L2)} \qquad (5\text{-}2)$$

the relation for the understeer coefficient becomes:

$$K_{US} = \frac{W\ L2}{C_{AF}\ (L1 + L2)} - \frac{W\ L1}{C_{AR}\ (L1 + L2)} \qquad (5\text{-}3)$$

where:

K_{US} = the understeer coefficient;

C_{AF} = the front cornering stiffness, (left + right);

C_{AR} = the rear cornering stiffness, (left + right);

W_F = the weight supported by the front wheels;

W_R = the weight supported by the rear wheels;

W = vehicle total weight;

$L1$ = CG to front axle distance; and

$L2$ = CG to rear axle distance.

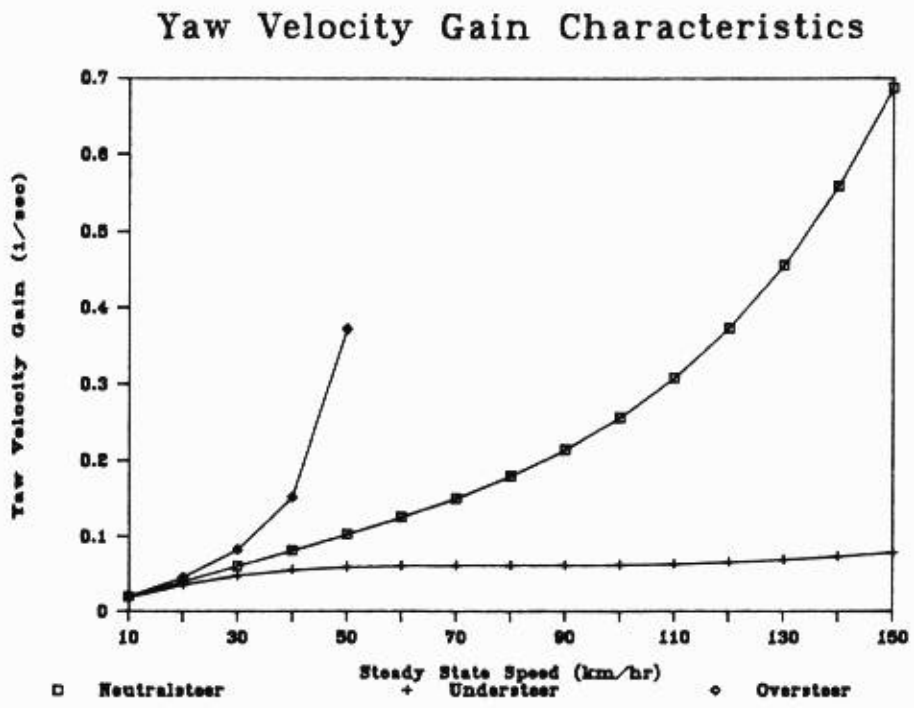

Figure 5-3 Weight distribution effect on yaw gain - predicted

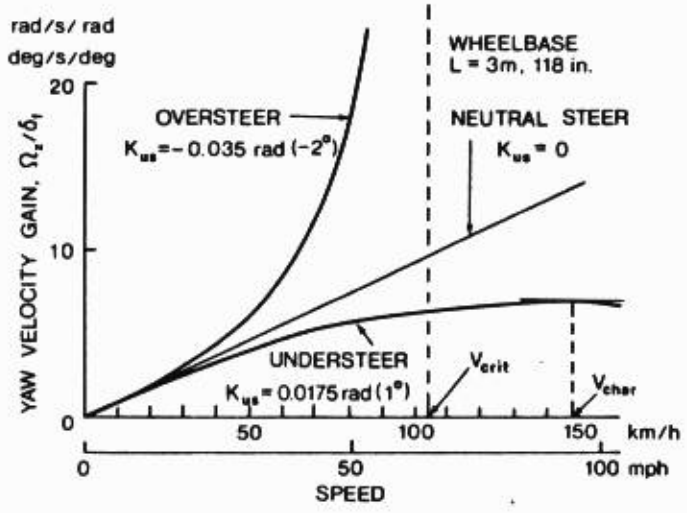

Figure 5-4 Vehicle yaw gain characteristics - Wong [3]

The understeer coefficient has the following significance to handling characteristics:

if Kus < 0.0 then, the vehicle will oversteer;

if Kus = 0.0 then, the vehicle will neutralsteer; and

if Kus > 0.0 then, the vehicle will understeer.

Therefore, both Wong's results and the simulation results correlate when equation (5-3) is calculated for each of the three cases simulated:

1) as prescribed in Table 2 Kus = -0.009

2) moving the C.G. forward Kus = 4.269

3) moving the C.G. rearward Kus = -4.359

In summary, the model generated for combined maneuver analysis correlates with previously cited results in the case of pure cornering. Next, the same model with a linear tire and suspension is used in actual combined maneuver analyses.

5.3 Basic Combined Maneuver Analysis

Combined maneuver analysis is performed by rotating the THETA vector (first explained in the beginning of Chapter Three) through 180 degrees. This will produce solutions starting with pure tractive effort through combined tractive/cornering effort to pure cornering continuing with braking/cornering and finally ending with pure braking effort. This simulation differs from the first because only the prescribed weight distribution is used. Also, the acceleration magnitude and steady-state velocity are held constant. The turn radius is derived from these constant values and will change for each value of THETA. Shown

below is typical output for one solution (one value of THETA). This particular output is for a THETA angle of 48°.

THE FINAL VALUES FOR THE SOL'N AFTER 6 ITERATIONS ARE:

**********ITERATED VARIABLES:

SIDESLIP ANGLE .....(RAD)....(BETA)=>-.0178587578

THE STEER ANGLE (FRONT ONLY) .....(RAD).....(DEL)=> .0033073964

Y DIR FORCE AT FRONT LEFT.....(NEWTONS).(FYTFL)=> 684.7306660

Y DIR FORCE AT FRONT RIGHT.....(NEWTONS).(FYTFR)=> 685.9106788

Y DIR FORCE AT BACK LEFT.....(NEWTONS).(FYBL)=> 932.5565782

Z DIR FORCE AT BACK LEFT.....(NEWTONS).(FZBL)=>-3432.715880

**********INTERNAL VARIABLES:

X DIR FORCE AT FRONT LEFT.....(NEWTONS).(FXTFL)=> 0

X DIR FORCE AT FRONT RIGHT.....(NEWTONS).(FXTFR)=> 0

X DIR FORCE AT BACK LEFT.....(NEWTONS).(FXBL)=> 848.1645976

X DIR FORCE AT BACK RIGHT.....(NEWTONS).(FXBR)=> 848.1645976

Y DIR FORCE AT BACK RIGHT.....(NEWTONS).(FYBR)=> 925.2038122

Z DIR FORCE AT FRONT LEFT.....(NEWTONS).(FZFL)=>-2508.20703

Z DIR FORCE AT FRONT RIGHT.....(NEWTONS).(FZFR)=>-2331.069275

Z DIR FORCE AT BACK RIGHT.....(NEWTONS).(FZBR)=>-3280.032041

SLIP ANGLE AT FRONT LEFT.....(RAD)....(ALFFL)=>-1.92134D-02

SLIP ANGLE AT FRONT RIGHT.....(RAD)....(ALFFR)=>-1.92466D-02

SLIP ANGLE AT BACK LEFT.....(RAD)....(ALFBL)=>-1.92627D-02

SLIP ANGLE AT BACK RIGHT.....(RAD)....(ALFBR)=>-1.92302D-02

SPIN. TO C.G. VERT DIST AT FRONT LEFT..(CM)..(HFL)=> 7.303433455

SPIN. TO C.G. VERT DIST AT FRONT RIGHT.(CM)..(HFR)=> 7.211603583

```
SPIN. TO C.G. VERT DIST AT BACK LEFT...(CM)..(HBL)=> 7.782430464
SPIN. TO C.G. VERT DIST AT BACK RIGHT..(CM)..(HBR)=> 7.703311703
SPINDLE TO GROUND  DIST AT FRONT LEFT..(CM).(ZSFL)=> 1.229665131
SPINDLE TO GROUND  DIST AT FRONT RIGHT.(CM).(ZSFR)=> 1.207846259
SPINDLE TO GROUND  DIST AT BACK LEFT...(CM).(ZSBL)=> 1.778609140
SPINDLE TO GROUND  DIST AT BACK RIGHT..(CM).(ZSBR)=> 1.699492378
ROLL ABOUT THE X AXIS.............(RAD)...(PHI)=>-3.357360206D-03
PITCH ABOUT THE Y AXIS.......... (RAD).(PITCH)=>-3.970537381D-02
SPRUNG MASS VERTICAL DEFLECTION......(CM).....(ZC)=> 13.99615267
TOTAL LATERAL LOAD TRANSFER DISTRIB .(NONE)(TLLTD)=> .5371154151
UNDERSTEER COEFFICIENT...............(RAD).(USCOEF)=>-.2744965791
VELOCITY BODY FIXED  X  DIR ....(CM/SEC).....(U)=> 3128.60480264
VELOCITY BODY FIXED  Y  DIR ....(CM/SEC).....(V)=> 55.8708249571

   AFTER CONVERGENCE THE FUNCTIONS SHOULD ALL BE ZERO THEY ARE:
F1= 5.92312458365D-04 F2=-2.8131438397D-03 F3=-3.565346219147D-06
F4=-3.26823178653D-06 F5=-1.15310217552D-06 F6= 9.32993103219D-06

AFTER CONVERGENCE, CORRECTION FACTORS SHOULD BE ZERO,THEY ARE:
B1= 1.85865427569D-06 B2=-3.99627459579D-06 B3=-8.81125149764D-06
B4= 7.36685859422D-11 B5= 1.27746063825D-10 B6=-1.45936560576D-06
```

As tabulated above, first the iterated variables used in the Newton Raphson routine are listed. Second, the derived and finally the auxiliary variables are given. This is the output for one solution of the vehicle model and many interesting facts can be documented from one solution. The longitudinal forces are zero at the front and equal at the back, indicating the enforced

rear wheel drive constraint (for this non-braking condition). The vertical and lateral forces are larger on the left side which is consistent with traversing a right hand turn, and so on. A series of these solutions as a function of the acceleration-magnitude direction (THETA) can more readily give information about a vehicles combined maneuver capabilities.

5.3.1 Steer Angle

Figure 5-5, 5-6, and 5-7 show steer angle (DELTA) characteristics during various conditions of combined longitudinal and lateral acceleration loads. Figure 5-5 shows as lateral acceleration increases (THETA approaches 90 degrees) for a given acceleration magnitude, the steer angle increases; although this is not as straight forward as analyzing the pure cornering case, this trait still indicates an understeer vehicle. The steer angle also increases as the acceleration magnitude increases, as seen the figures. Also, for a given acceleration magnitude and direction, the steer angle decreases for an increase in steady state velocity. This is seen by comparing all three figures. These steer characteristics are understood easier by inspection of equation 3-9. This equation shows that the turn radius (RHO) is a function of lateral acceleration and steady-state velocity. So, for constant lateral acceleration, as velocity increases, the turn radius increases, and the steer angle decreases. The converse is true for increases in lateral acceleration, (A sin(THETA)), the steer angle becomes larger.

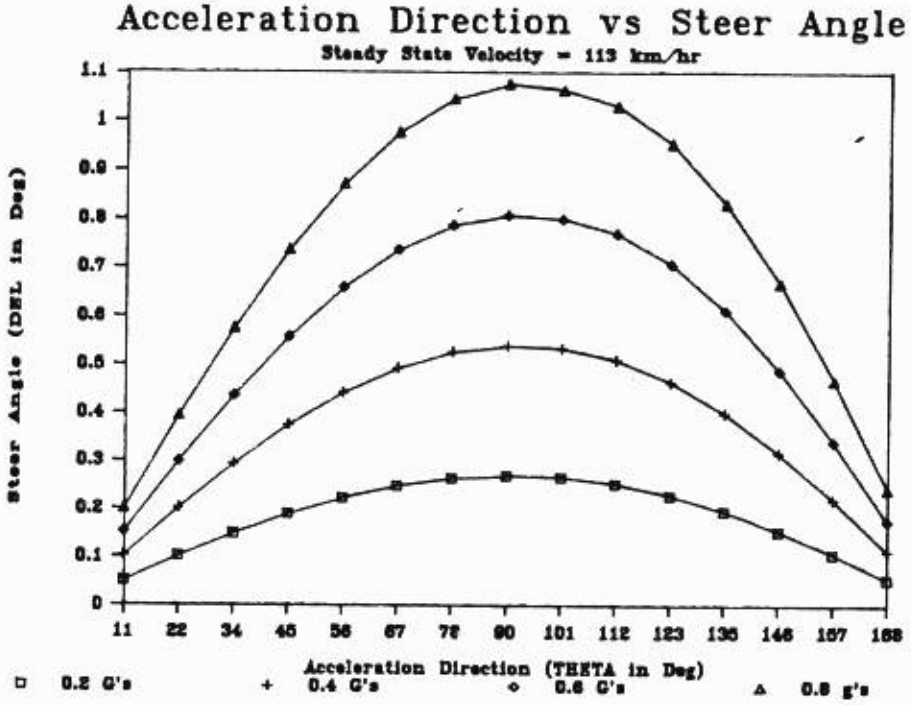

Figure 5-5 Steer angle characteristics for 113 km/hr

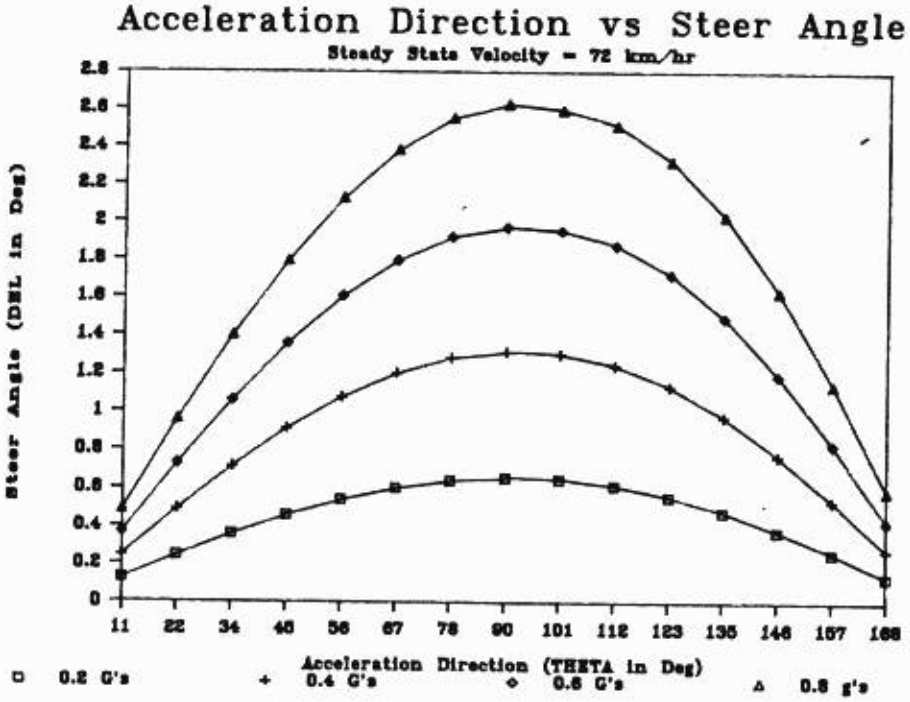

Figure 5-6 Steer angle characteristics for 72 km/hr

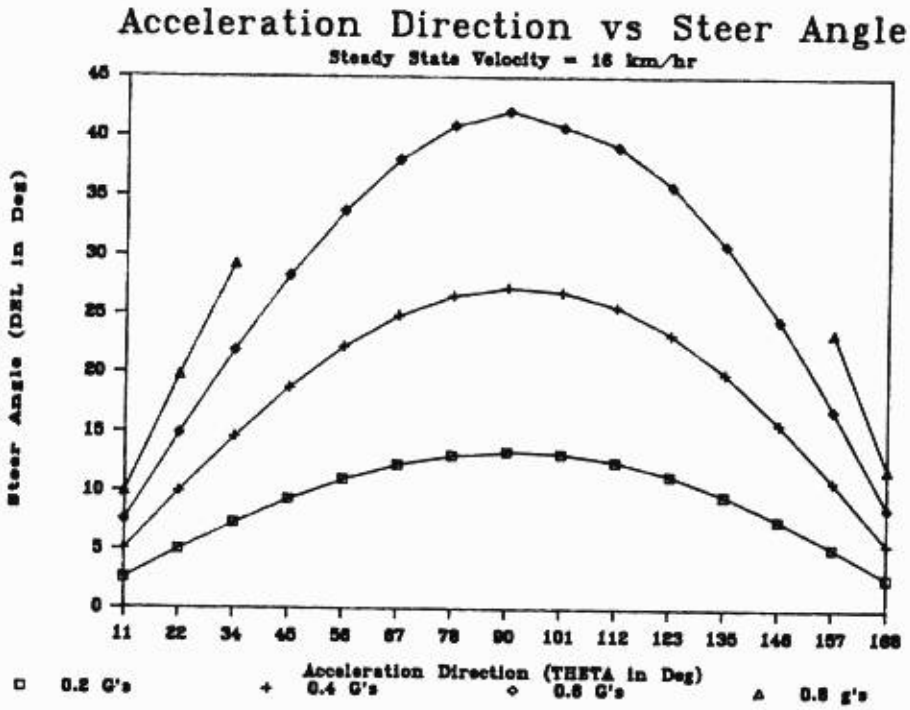

Figure 5-7 Steer angle characteristic for 16 km/hr

5.3.2 Longitudinal Spindle Forces

Figures 5-8, and 5-9 show the longitudinal spindle forces. During the tractive cases (THETA = 0 to 90) the front forces are zero and during the braking conditions (THETA = 90 to 180) the front forces are 70% of the total stopping force as prescribed by the BP parameter. As seen in the figures the longitudinal forces are independent of steady state velocity. The longitudinal forces go up linearly with the acceleration magnitude (not shown in the figures) which is the result of using a linear tire model with no saturation characteristics. These traits are indicative of the rear wheel drive constraint being imposed.

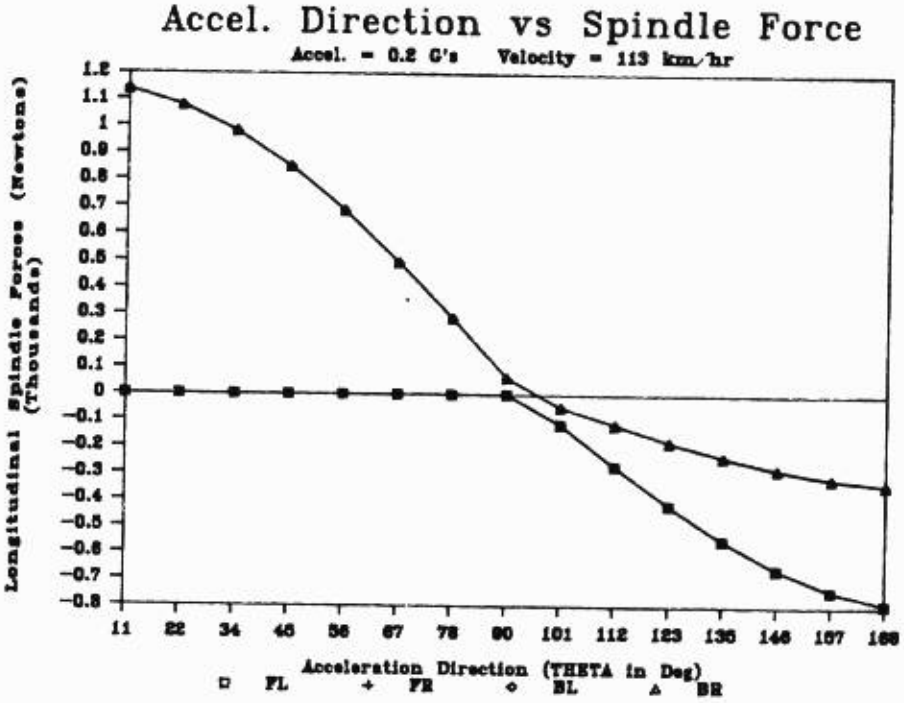

Figure 5-8 Longitudinal forces for 113 km/hr and 0.2 G's

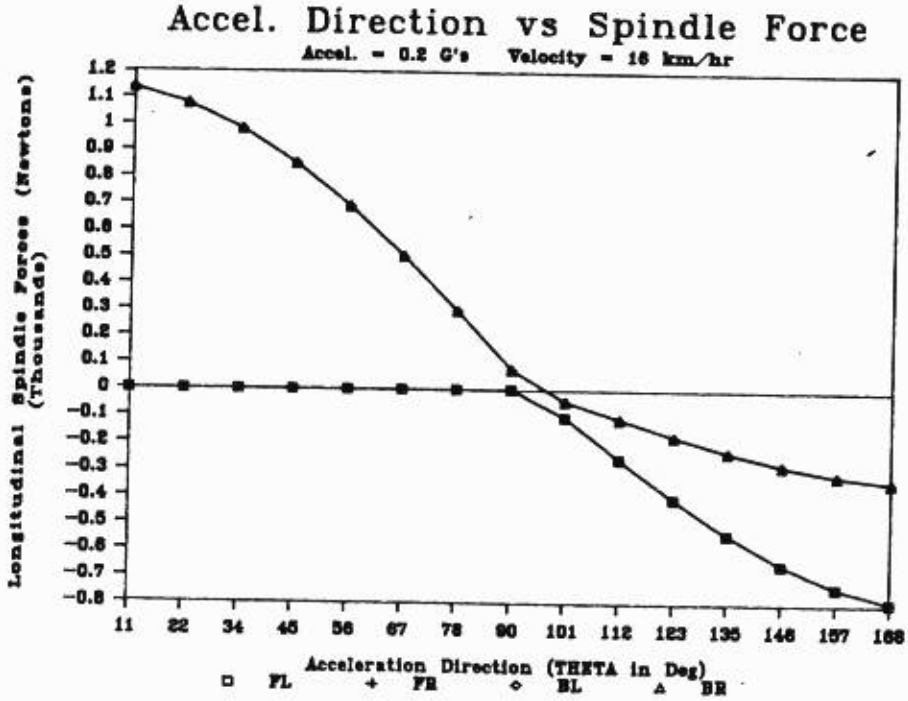

Figure 5-9 Longitudinal forces for 16 km/hr and 0.2 G's

5.3.3 Slip Angles and Lateral Spindle Forces

Figures 5-10, thru 5-17 show the slip angles and the lateral spindle forces for different steady-state velocities and acceleration magnitudes. As the lateral component of the acceleration magnitude increases, more lateral force must be reacted by the tires. Therefore, the slip angles and lateral forces must become larger, as seen in the figures. The figures show at high speeds the slip angles (and therefore the lateral forces) are relatively equal and vary at low speeds. This is somewhat misleading because the slip angle magnitudes are influenced by the turn radius, similarly to the steer angle (see section 5.5.1). At high speeds the turn radius is large compared to the vehicle geometry therefore, the slip angles are relatively equal side to side, see Figures 5-10 and 5-11. However, at a lower speed (lower turn radius) the differences between the slip angles are more readily discernable, see Figures 5-12 and 5-13. Also, the relative equality of the slip angles front to rear is attributable to the nearly neutralsteering characteristic of this particular vehicle. The fact that a linear tire model with no normal load roll-off is used also influences these conditions. This linear condition means there are no surprises when the lateral forces are seen in figures 5-14 thru 5-17. In fact, the lateral force plots only look different from the slip angle plots because of the difference between the tire cornering stiffnesses from front to back.

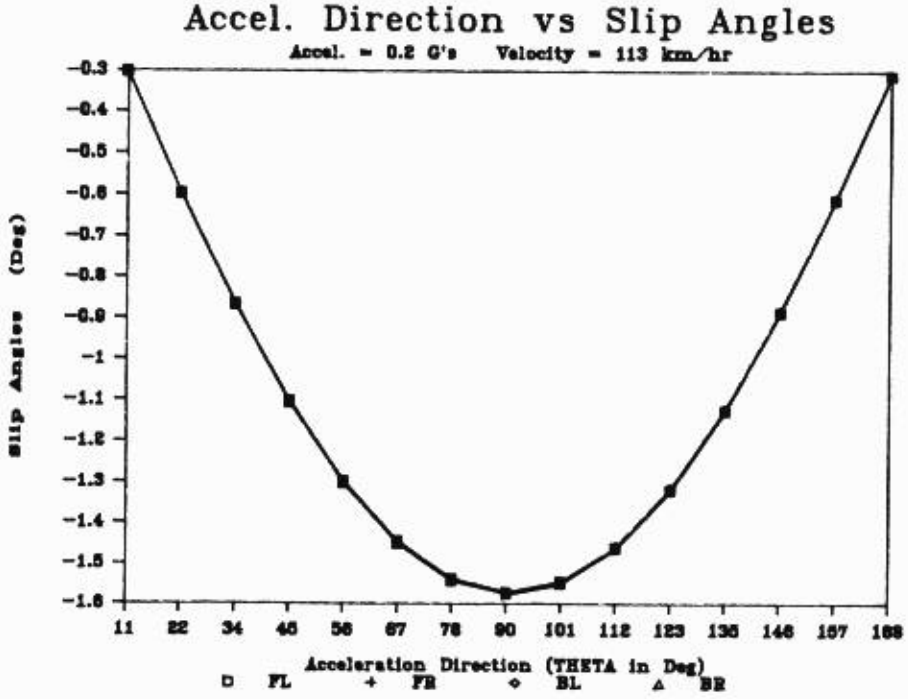

Figure 5-10 Slip angles for 113 km/hr and 0.2 G's

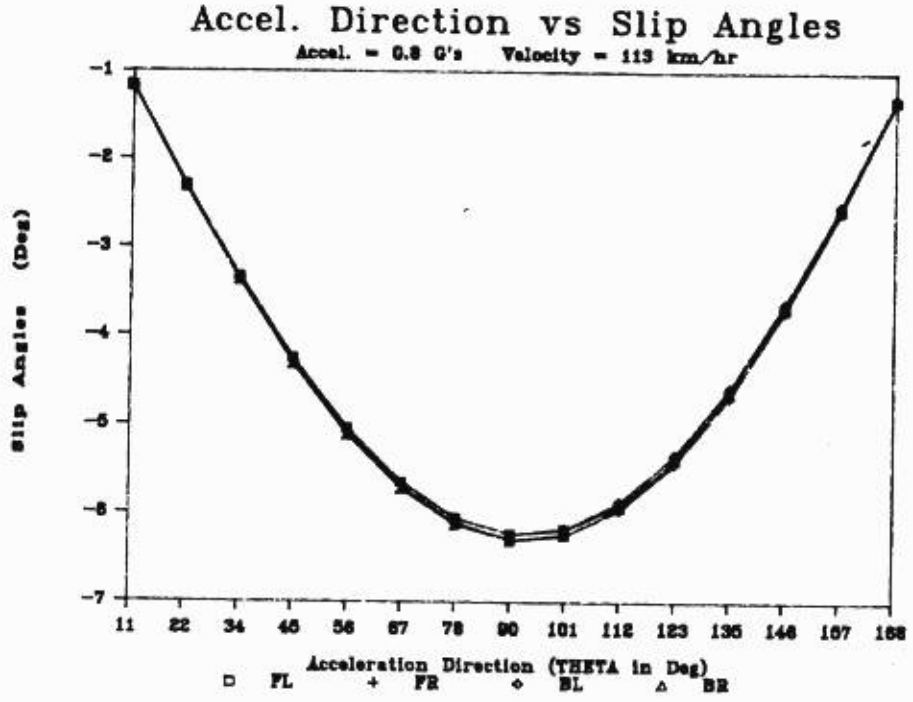

Figure 5-11 Slip angles for 113 km/hr and 0.8 G's

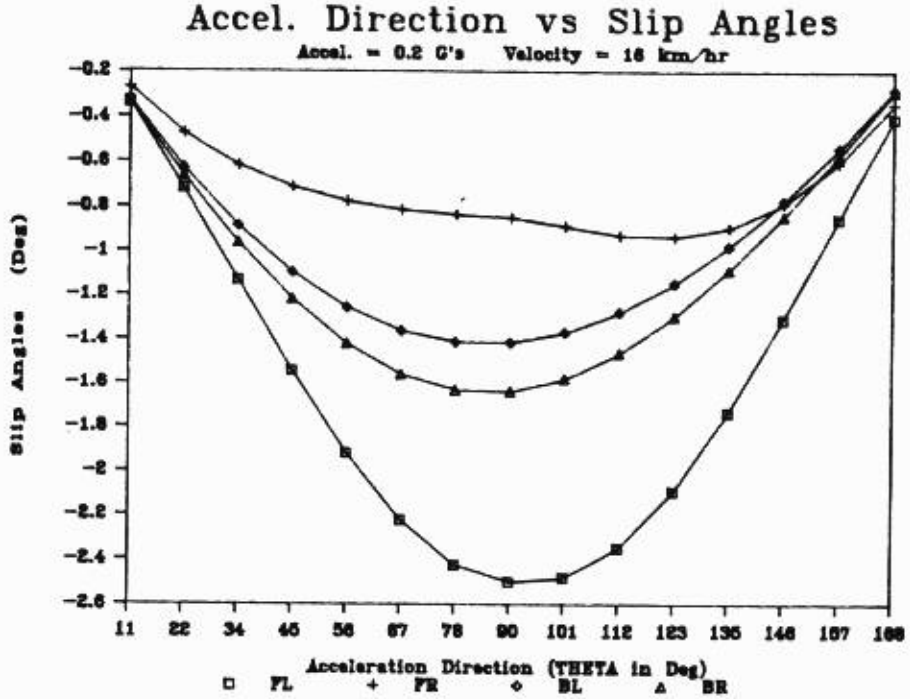

Figure 5-12 Slip angles for 16 km/hr and 0.2 G's

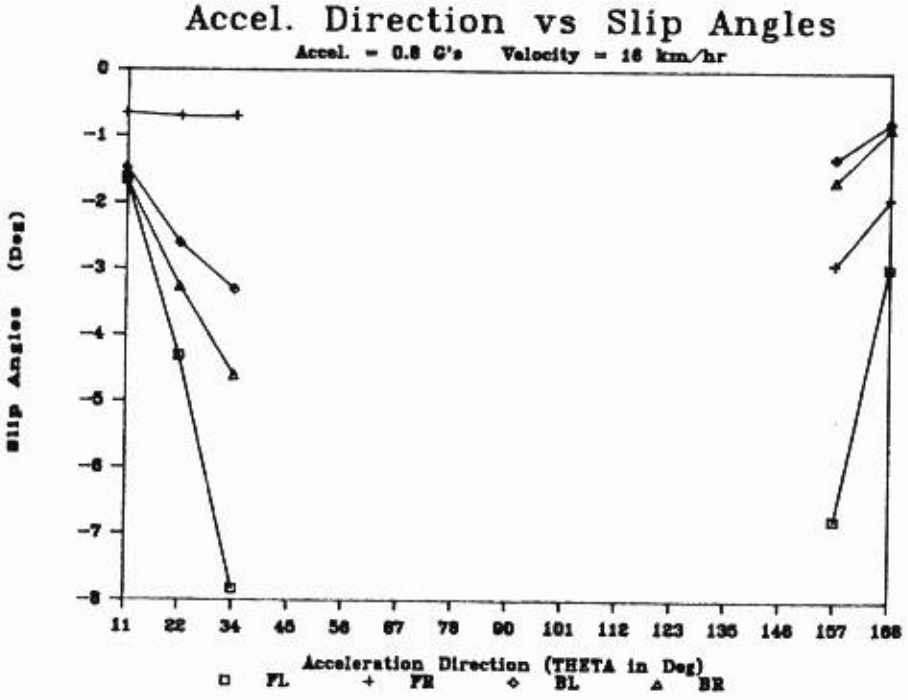

Figure 5-13 Slip angles for 16 km/hr and 0.8 G's

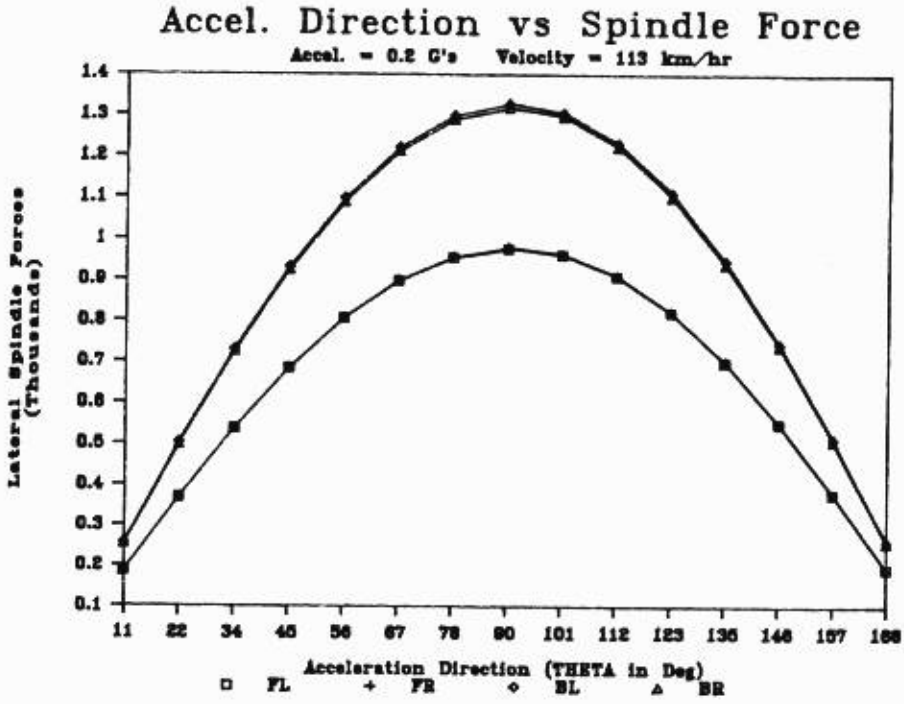

Figure 5-14 Lateral forces for 113 km/hr and 0.2 G's

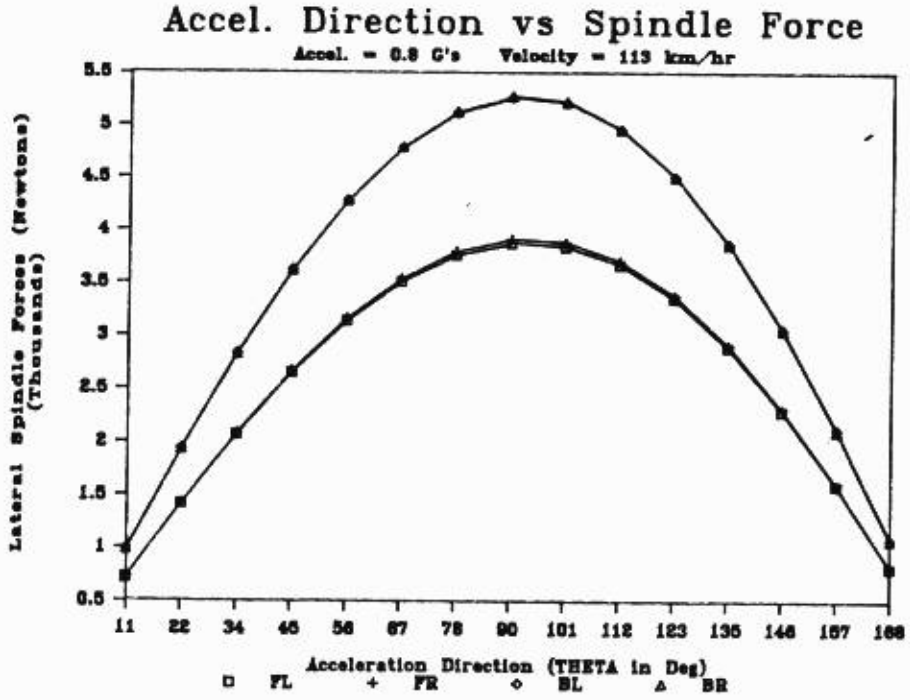

Figure 5-15 Lateral forces for 113 km/hr and 0.8 G's

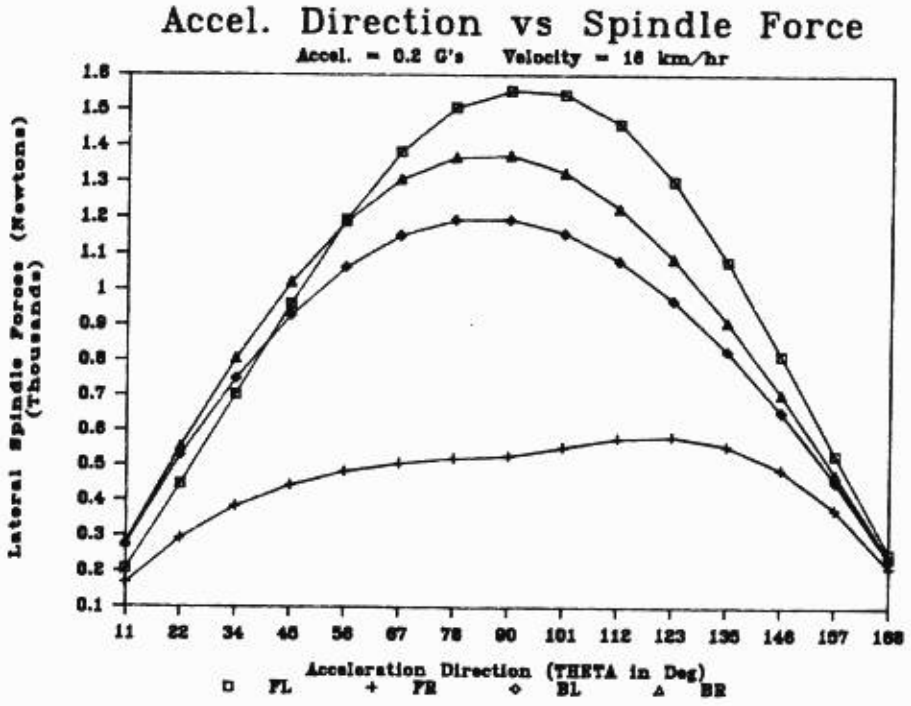

Figure 5-16 Lateral forces for 16 km/hr and 0.2 G's

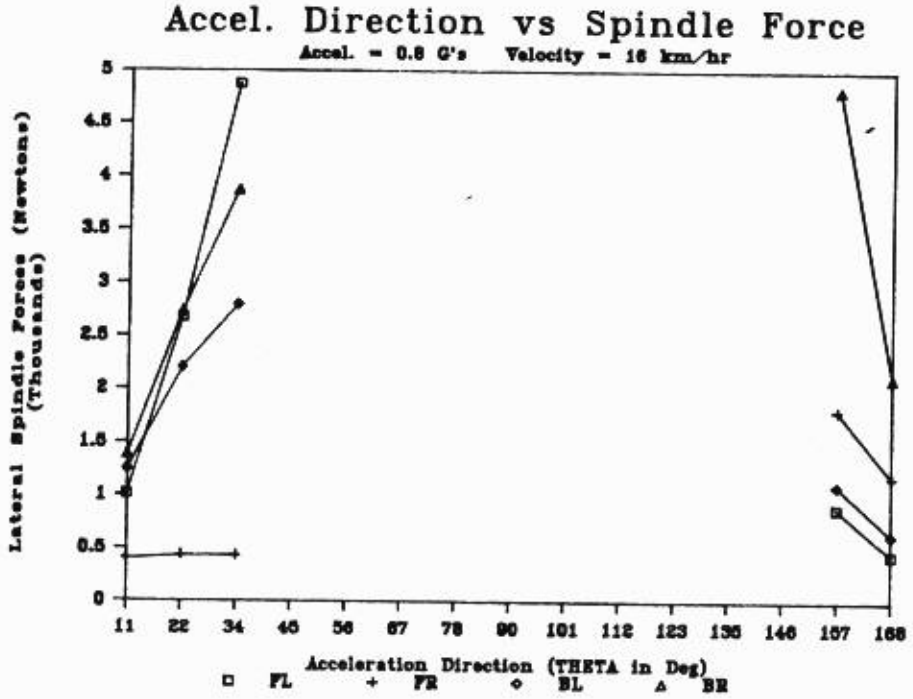

Figure 5-17 Lateral forces for 16 km/hr and 0.8 G's

5.3.4 Vertical Spindle Forces

Figures 5-18, 5-19, 5-20, and 5-21 show the vertical spindle forces for different steady-state velocities. These figures show that lateral weight transfer is constant for a given lateral acceleration, regardless of velocity. Also, the left side forces are greater, which indicates motion around a right hand turn. The back forces are greater because of the weight bias of this vehicle. A plot of vertical spindle displacements look precisely the same as the forces with a different Y axis so they will not be presented here.

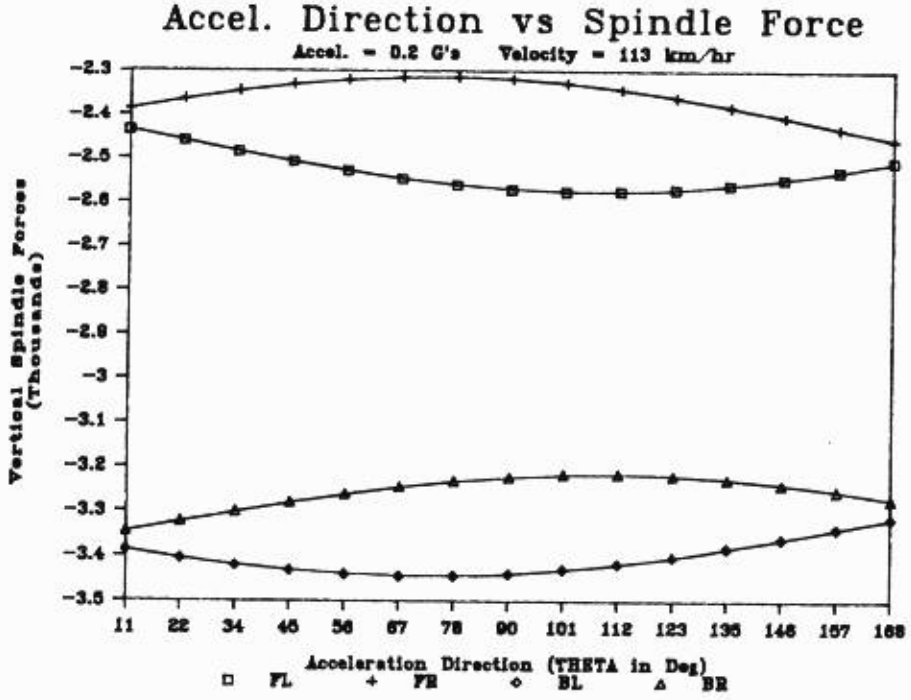

Figure 5-18 Vertical forces for 113 km/hr and 0.2 G's

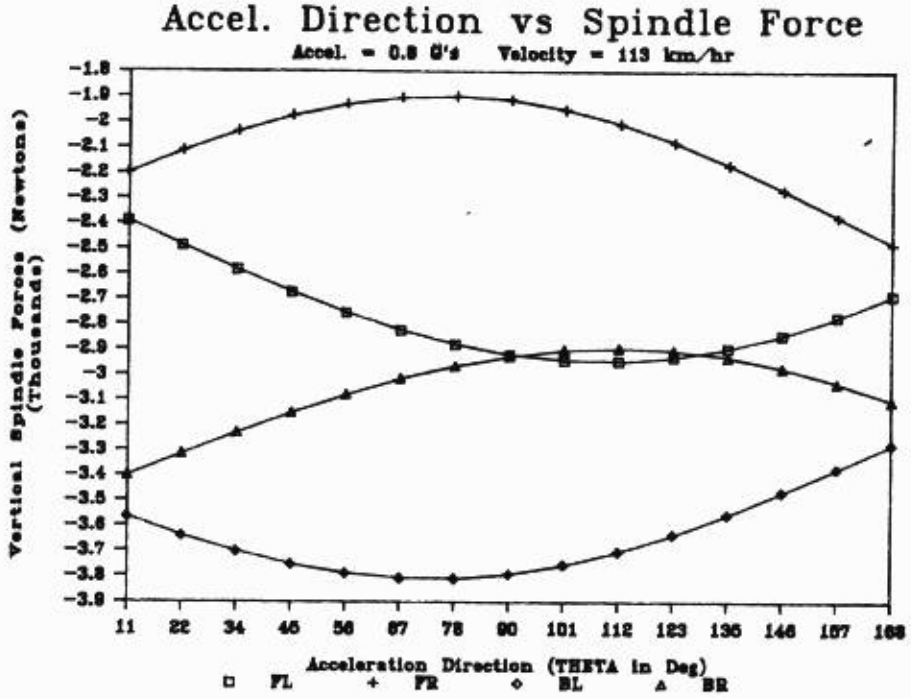

Figure 5-19 Vertical forces for 113 km/hr and 0.8 G's

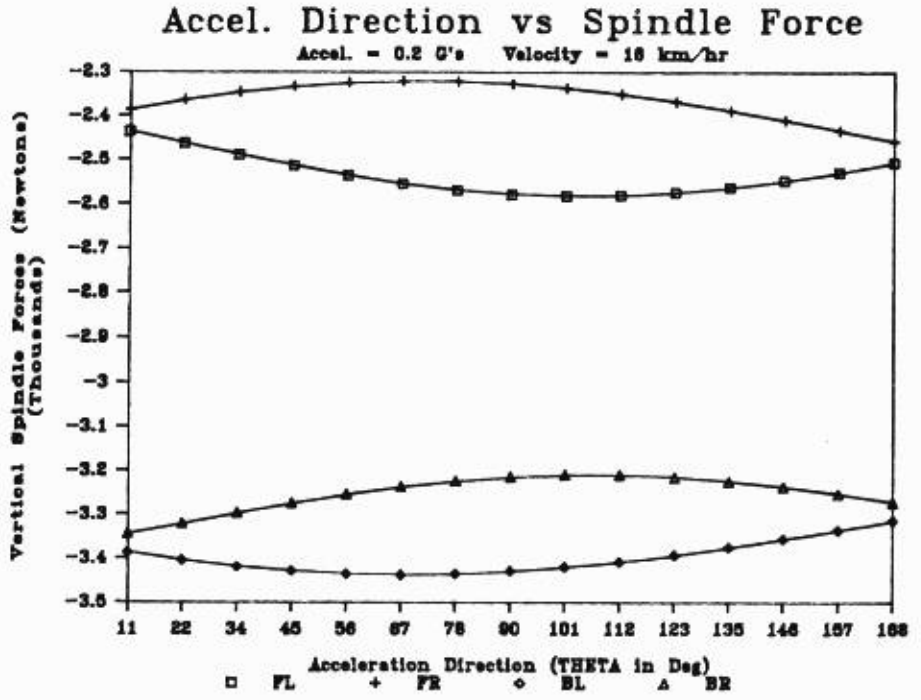

Figure 5-20 Vertical forces for 16 km/hr and 0.2 G's

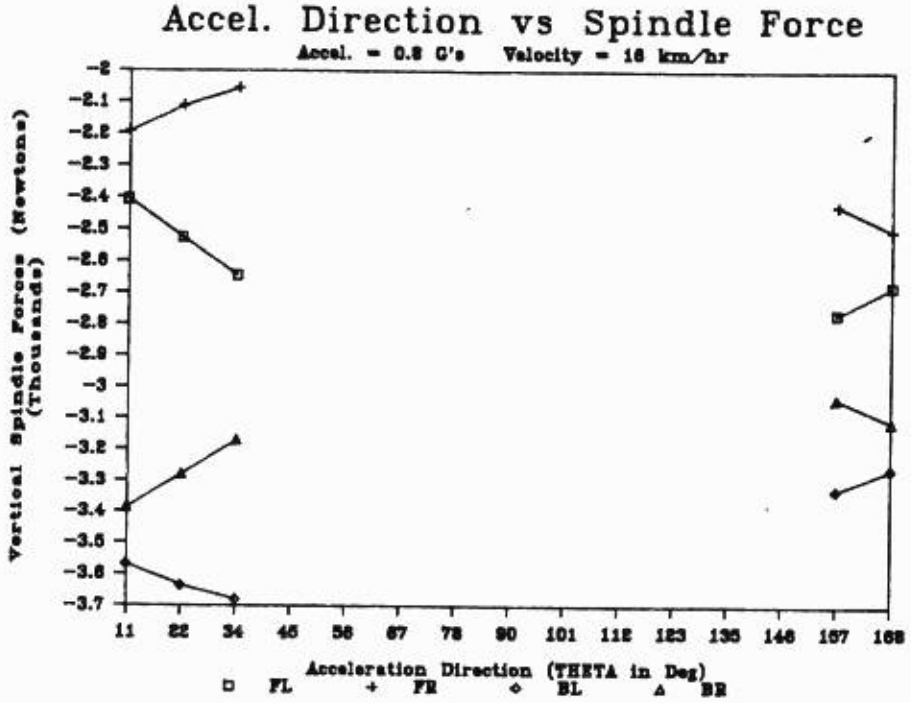

Figure 5-21 Vertical forces for 16 km/hr and 0.8 G's

5.3.5 Vehicle Rotation Angles

Figures 5-22, 5-23, 5-24, and 5-25 show vehicle rotations during combined maneuvers. The pitch angle starts negative and increases as the acceleration magnitude rotates to a pure deceleration direction. The reason that the pitch angle starts negative is due to the static deflection characteristic of the vehicle which is not accounted for in the vehicle equations. The total excursion of the pitch angle increases with acceleration magnitude. The roll angle (PHI) begins at zero, moves to maximum at pure cornering, and returns to zero as expected. The maximum roll angle reached at pure cornering is larger for increasing values of acceleration magnitude. The side slip angle, BETA, is

positive for low values of steady-state velocity and negative for high values of steady-state velocity. The magnitude of acceleration has no effect on this behavior. This is consistent with the pure cornering analysis done in section 5.2 because this vehicle slightly oversteers at the limit (neg. BETA implies oversteer, see section 2.3). The magnitude of the negative angle also depends on the fact that the coordinate origin is not in the geometric center of the vehicle, but at the center-of-gravity. Therefore, if the results for this vehicle are plotted, and BETA is measured from the center of the vehicle, then the magnitude of BETA would be more positive for all cases, indicating slightly less oversteer.

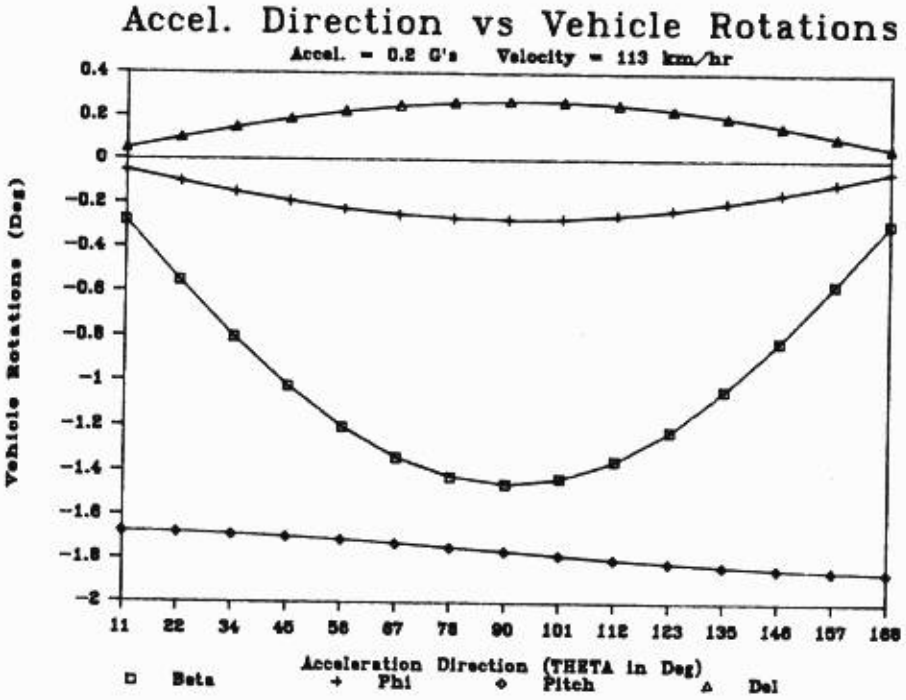

Figure 5-22 Vehicle rotations for 113 km/hr and 0.2 G's

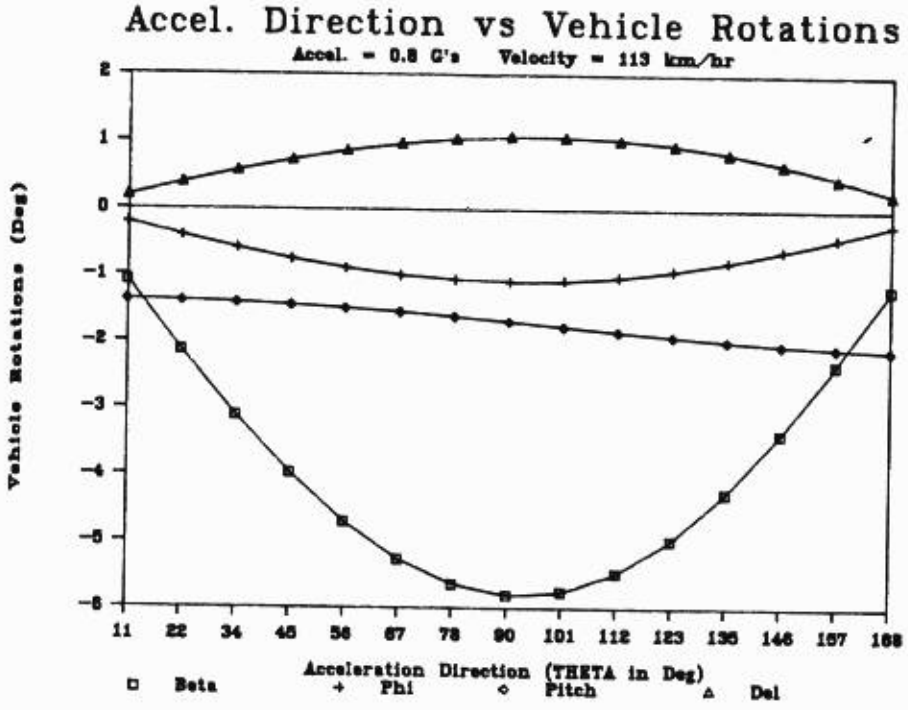

Figure 5-23 Vehicle rotations for 113 km/hr and 0.8 G's

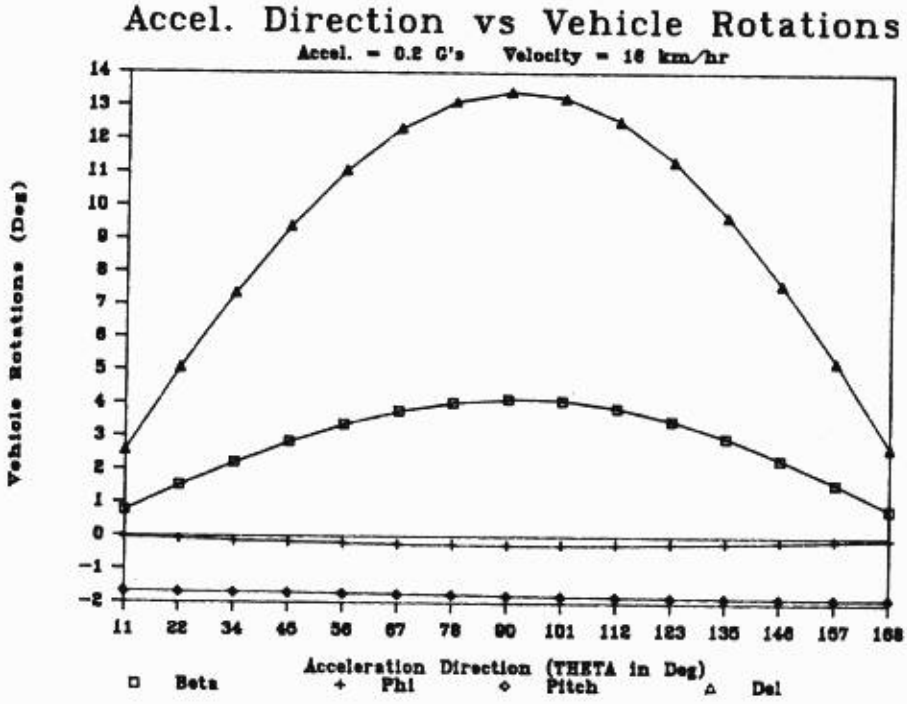

Figure 5-24 Vehicle rotations for 16 km/hr and 0.2 G's

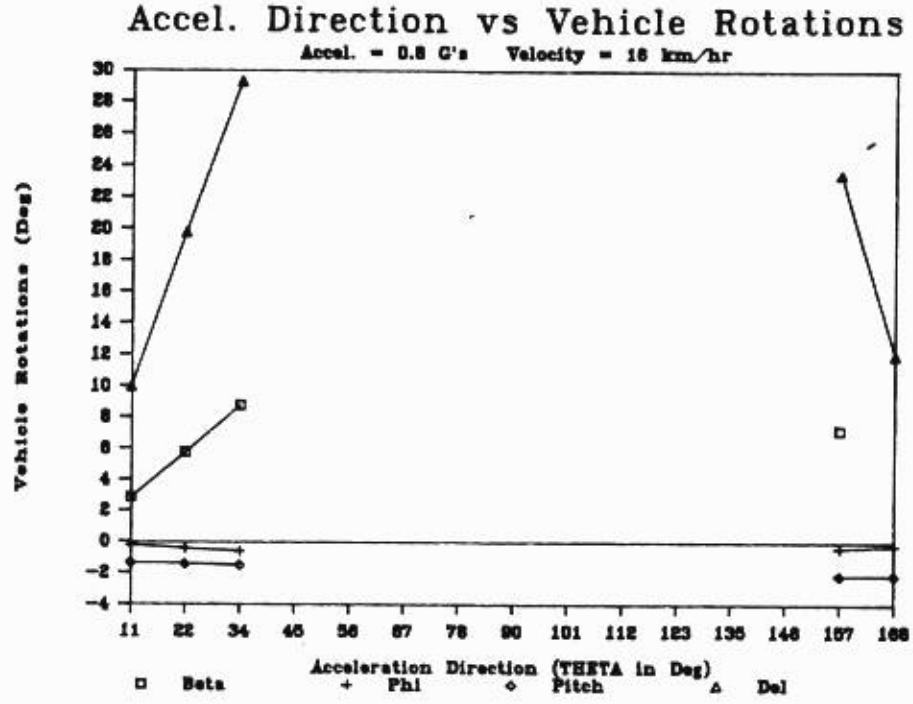

Figure 5-25 Vehicle rotations for 16 km/hr and 0.8 G's

5.3.5 Basic Combined Maneuver Analysis Summary

The results presented in section 5.3 above correspond to what would be expected from this particular vehicle. The results also demonstrated some of the limitations of the Newton Raphson iteration technique. These limitations are demonstrated by the inability of the program to converge at high acceleration magnitudes and low steady state-velocities. This behavior is actually correct for the vehicle because it is difficult to obtain high G's at low speeds. However, because the tire model is linear the solutions should have converged. A non-linear tire model could demonstrate this behavior.

5.4 Combined Maneuver Analysis with a Nonlinear Tire Model

The same analysis as performed in section 5.3 was attempted using the non-linear tire model described by equations (3-59) to (3-66). The addition of this tire model to the total vehicle, increased the non-linearity of the system significantly. Therefore, the Newton Raphson solution scheme becomes unstable. Attempts to remedy this condition include:

1. Calculation of the initial guess based on input to start closer to the final solution for each value of THETA.
2. Reset divergent unknowns when they were larger than practically possible.
3. Calculate the Newton Raphson derivative step based on the magnitude of the unknowns.
4. Allow the derivative step to be manually changed during the execution of the model.

These changes to the solution scheme allow a portion of the linear range solutions to converge. A representative amount of the data from these solutions are shown in Figures 5-26 and 5-27. Comparison of these figures to Figures 5-24 and 5-16 shows that the non-linear tire solutions are the same as the linear tire solutions; which they should be in the linear range of vehicle operation. The insufficiencies of the Newton Raphson scheme for this system of equations are discussed below.

The limitations of the model in the most severe case involves the inability for the simulation to converge at the borderline regions of linear vehicle operation. The Newton Raphson

iteration technique is known for its fast convergence with monotonically nonlinear problems or cases where the initial guess can be predicted close to the final solution. However, with cyclically non-linear problems the solution can easily diverge and oscillate around a local minimum not near the solution. Another condition known as the newton trap occurs when the solution oscillates around the solution. In the case of this vehicle model both conditions occurred at the borderline solutions. The Newton Raphson technique was used in this work because of its convergence characteristics, but most of all, because of its ease of implementation without the need for external software. More can be learned about the interaction between the functions when the internal workings of the solver can be monitored. The convergence (at all) of the vehicle model with the nonlinear tire is attributable to this monitoring.

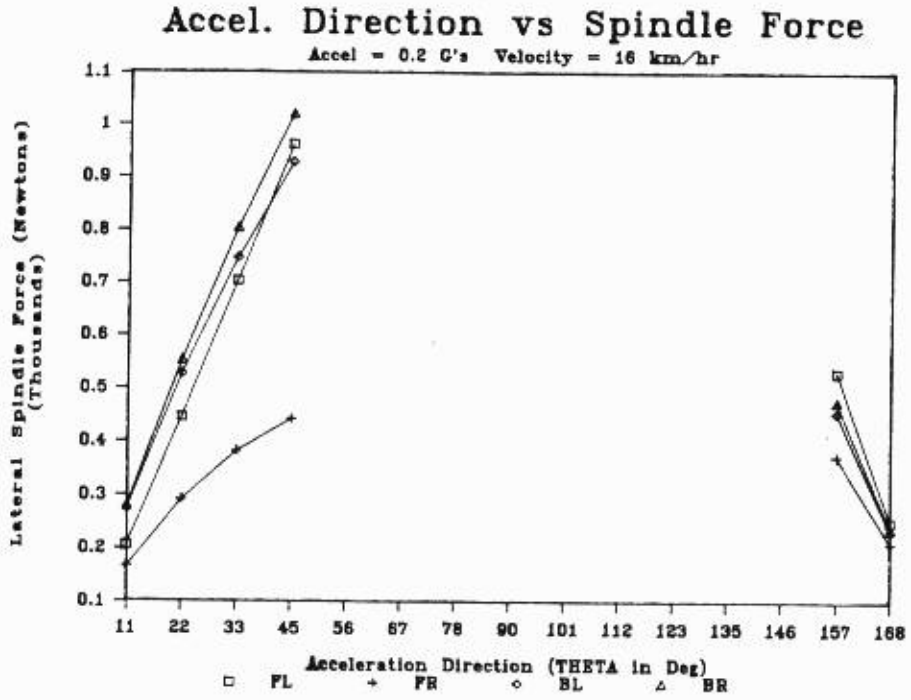

Figure 5-27 Lateral force for 113 km/hr and 0.2 G's with a nonlinear tire model

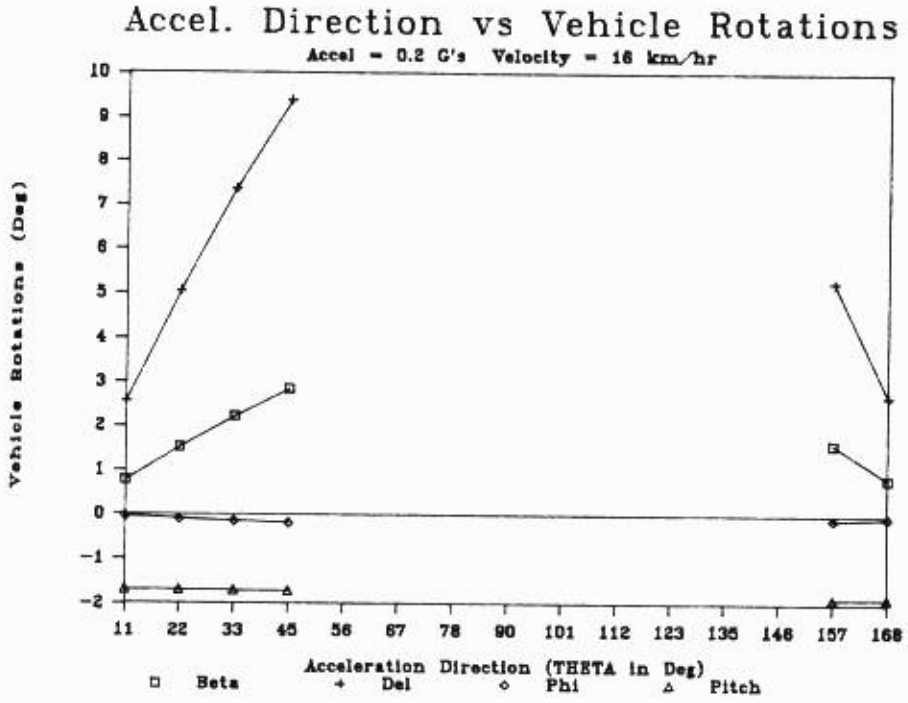

Figure 5-26 Vehicle rotations for 113 km/hr and 0.2 G's with a nonlinear tire model